ACS OMEGA

Article

Cite This: ACS Omega 2018, 3, 3165−3172

Single-Molecule Nonresonant Wide-Field Surface-Enhanced Raman Scattering from Ferroelectrically Defined Au Nanoparticle Microarrays

Rusul M. Al-Shammari,[†,‡] Nebras Al-attar,[*,†,§] Michele Manzo,[∥] Katia Gallo,[∥] Brian J. Rodriguez,[*,†,‡] and James H. Rice[*,†]

[†]School of Physics and [‡]Conway Institute of Biomolecular and Biomedical Research, University College Dublin, Belfield, D04 N2E5, Dublin, Ireland

[§]Laser and Optoelectronics Engineering Department, University of Technology, 10066 Baghdad, Iraq

[∥]Department of Applied Physics, KTH—Royal Institute of Technology, 106 91 Stockholm, Sweden

Supporting Information

ABSTRACT: Single-molecule detection by surface-enhanced Raman scattering (SERS) is a powerful spectroscopic technique that is of interest for the sensor development field. An important aspect of optimizing the materials used in SERS-based sensors is the ability to have a high density of "hot spots" that enhance the SERS sensitivity to the single-molecule level. Photodeposition of gold (Au) nanoparticles through electric-field-directed self-assembly on a periodically proton-exchanged lithium niobate (PPELN) substrate provides conditions to form well-ordered microscale features consisting of closely packed Au nanoparticles. The resulting Au nanoparticle microstructure arrays (microarrays) are plasmon-active and support nonresonant single-molecule SERS at ultralow concentrations ($<10^{-9}$−10^{-13} M) with excitation power densities $<1 \times 10^{-3}$ W cm^{-2} using wide-field imaging. The microarrays offer excellent SERS reproducibility, with an intensity variation of <7.5% across the substrate. As most biomarkers and molecules do not support resonance enhancement, this work demonstrates that PPELN is a suitable template for high-sensitivity, nonresonant sensing applications.

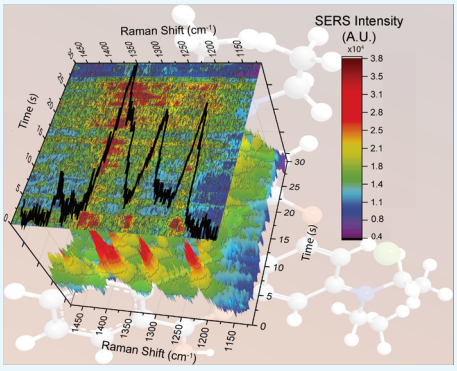

INTRODUCTION

Single-molecule (SM) surface-enhanced Raman scattering (SERS) is enabled by the large electromagnetic field enhancement "hot spots" that occur between closely packed nanoparticles. Thus, an objective in developing nanomaterials for single-molecule SERS is to prepare well-defined and reproducible nanoparticle assemblies that support the formation of a large number of hot spots.[1−3] Through ferroelectric nanolithography, static electric field distributions can be engineered in a ferroelectric crystal to direct bottom-up assembly and nanoparticle deposition at the surface.[3−6] This results in substrates with closely packed nanoparticles in well-defined and reproducible microstructure arrays (microarrays).[3−6]

Lithium niobate (LN) is a ferroelectric crystal that enables selective polarization-driven deposition of metallic nanoparticles due to its large reversible spontaneous polarization along the crystallographic *Z*-axis.[4,7] Electric-field poling and chemical patterning have been used to tailor surface charge and reactivity on a LN surface for the fabrication of metallic nanostructures.[8−11] Furthermore, LN has been shown to be cytocompatible with several cell lines and nanoparticles deposited on LN have been shown to support SERS.[7,12−19] Periodically proton-exchanged lithium niobate (PPELN) templates have been previously applied for directed self-assembly of silver (Ag) nanoparticles.[8,11] PPELN formed through one-dimensional chemical patterning of LN via proton exchange results in a surface with alternating PE and LN stripes.[8] Proton exchange of a LN surface through reactive ion-etched (RIE) mask openings results in lateral diffusion (LD) of protons under the mask and leads to RIE and LD regions in the PE area.[11,20−22] Gold (Au) nanoparticles have been shown to reduce from aqueous $HAuCl_4$ preferentially in RIE regions depending on the Au^{3+} ion concentration.[20]

In this work, the formation of microarrays of Au nanoparticles on PPELN (Au-PPELN) is shown to be applicable to nonresonant single-molecule SERS using wide-field imaging. The use of wide-field SERS imaging here aids in overcoming general obstacles in single-molecule SERS detection in standard micro Raman systems by increasing the spatial resolution limitation, the signal-to-noise ratio, and the imaged area of the sample to ∼20 × 20 μm^2, while also decreasing the acquisition time, which enables the detection of multiplexed SERS signals from probe molecules.[23,24] We demonstrate that Au-PPELN enables nonresonant single-molecule SERS using low probe

Received: September 1, 2017
Accepted: November 24, 2017
Published: March 15, 2018

DOI: 10.1021/acsomega.7b01285
ACS Omega 2018, 3, 3165−3172

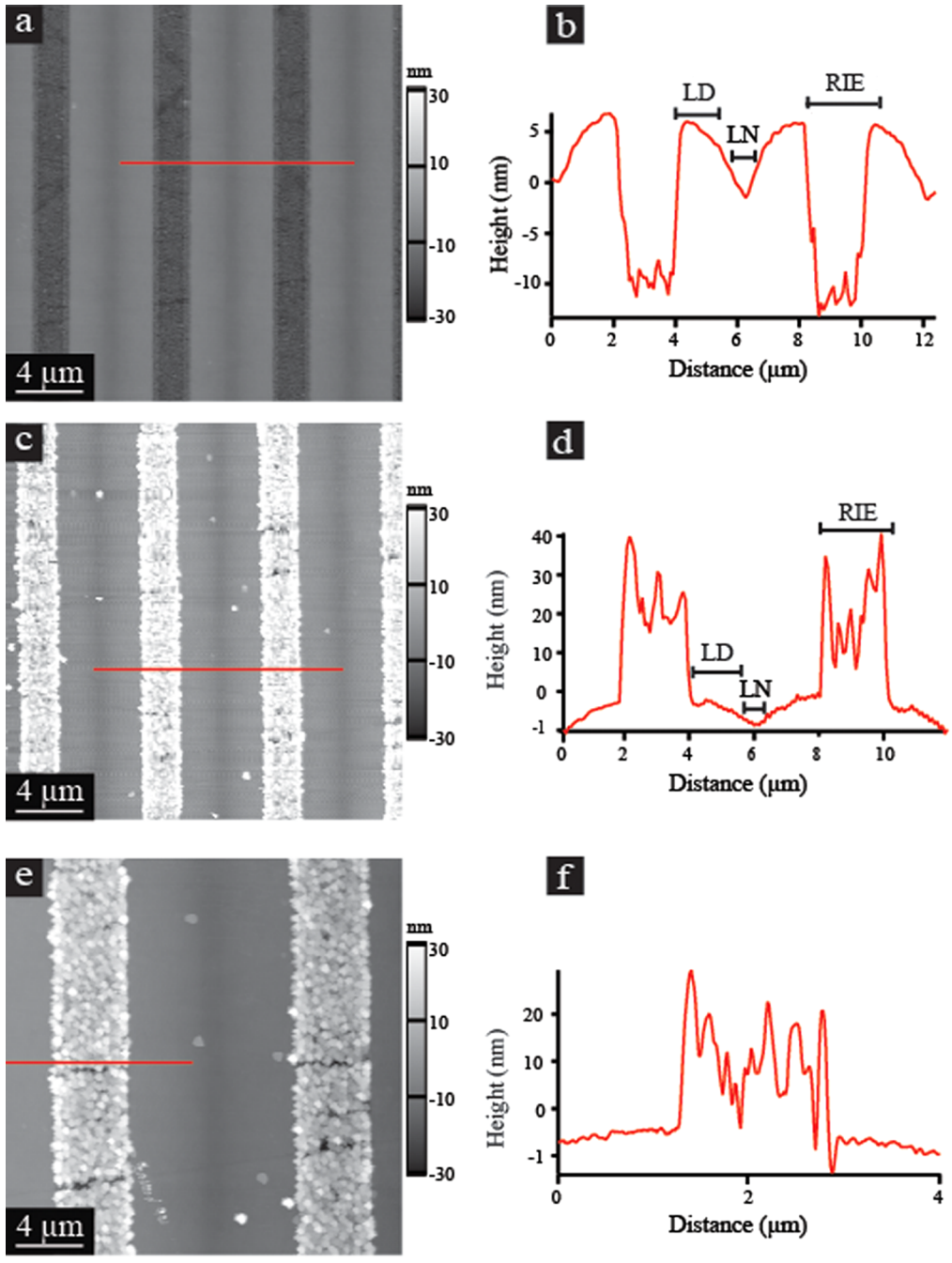

Figure 1. AFM topography and average line profile of (−Z) PPELN (a, b) prior to Au deposition and (c, d) after Au deposition; marked regions are lateral diffusion (LD), lithium niobate (LN), and reactive ion etching (RIE) of PPELN. (e) AFM topography image (10 μm × 10 μm area) of the (Au-PPELN) substrate showing the presence of Au nanoparticles in the RIE region and the corresponding AFM line scan is shown in (f).

molecule concentrations ($<10^{-9}$–10^{-13} M) and a low laser power density ($<1 \times 10^{-3}$ W cm^{-2}). The use of low power density aids in avoiding problematic photodegradation products, which are expected to have a SERS signal comparable to or even larger than the nonresonant target analyte.[25] Nonresonant single-molecule SERS detection is important in biodetection applications as most biomarkers and molecules do not support resonance enhancement.[26,27] Here, fluorescence imaging and fluorescence lifetime studies have been used to investigate the localization of the probe molecule at the Au-PPELN surface to establish that the substrate simultaneously supports surface fluorescence luminescence and SERS. This work demonstrates that Au-PPELN templates are suitable for high-sensitivity analytical applications.

RESULTS AND DISCUSSION

Atomic force microscopy (AFM) imaging of the PPELN surface was undertaken to determine the surface topography of the substrate's surface prior to the photodeposition of the Au nanoparticles (Figures 1a,b and S2, Supporting Information). The AFM topography image (Figure 1a) and corresponding line profile (Figure 1b) show topographical features assigned to the PE regions of the PPELN surface that comprise the central RIE region and the adjacent LD regions, as indicated in Figure 1b, the insertion of protons into the crystal lattice and resulting

DOI: 10.1021/acsomega.7b01285
ACS Omega 2018, 3, 3165−3172

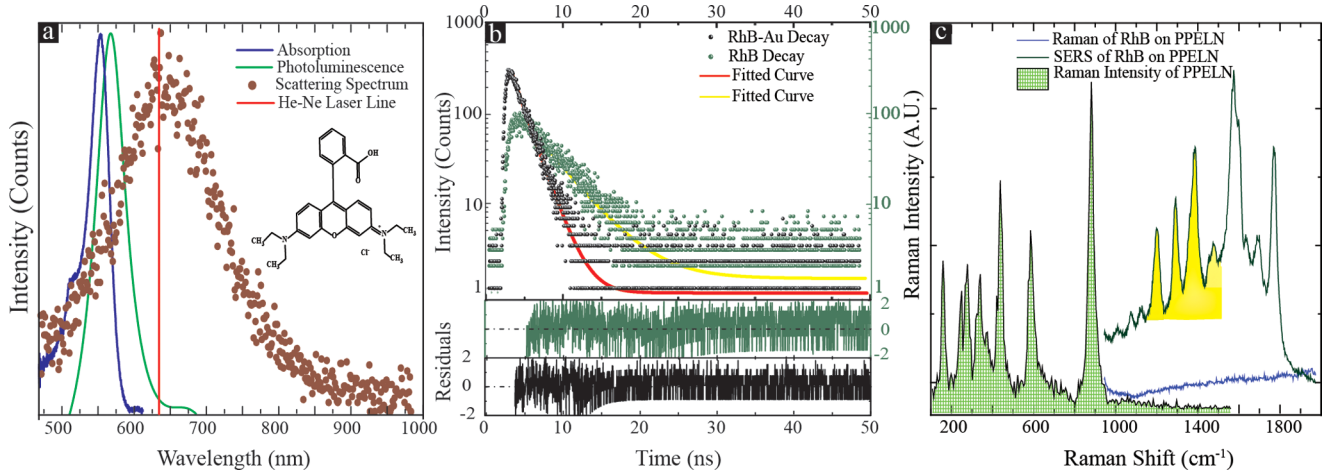

Figure 2. (a) Optical scattering spectrum (brown) from Au-PPELN substrate shown along with the optical absorption spectrum (blue) and fluorescence emission spectrum (green) from RhB deposited onto a (dielectric) glass slide. The insert shows a schematic of the molecular structure of the probe molecule. (b) Fluorescence lifetime studies recorded using a millimolar concentration of the probe molecule RhB on PPELN with and without Au. The lifetime decay trace of the fluorescence emission from Au-PPELN substrate with RhB showing a larger fluorescence signal intensity and a shortened lifetime compared with only PPELN with RhB. Single exponential fits to the decay traces are shown in red and yellow. A shortened lifetime (τ = 2.2 ns) was found for the Au-PPELN substrate with RhB compared with PPELN with RhB without Au nanoparticles (τ = 3.5 ns). The residual standard deviation indicates an average value close to 0. The observed fluorescence intensity array (yellow line) arising from areas of the substrate where Au is deposited. (c) SERS spectra recorded at 632.8 nm. The green region shows Raman bands arising from the PPELN substrate, which are below ~1000 cm^{-1}. The blue line shows the Raman spectrum above ~1000 cm^{-1} arising from PPELN with RhB, whereas the green line shows the SERS spectrum for RhB on an Au-PPELN surface. The yellow region shows the three peaks that we used to calculate the enhancement factor (EF).

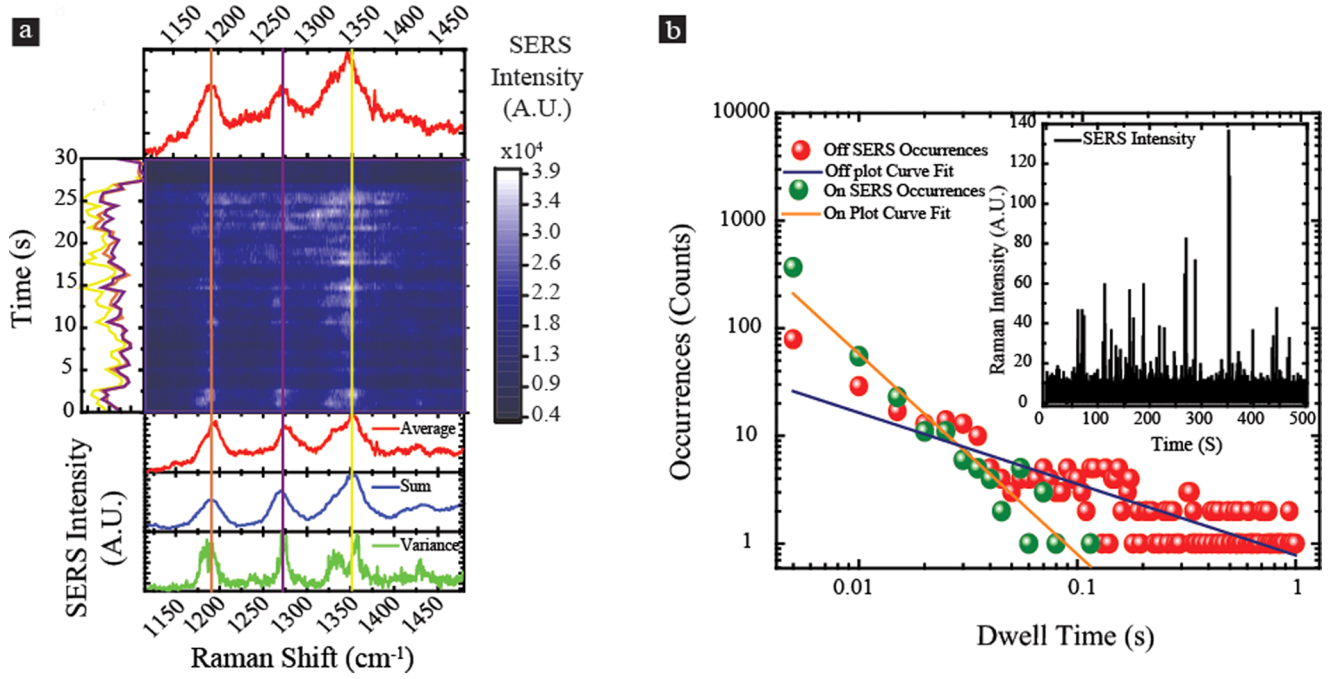

Figure 3. Nonresonant SERS from Au-PPELN with RhB, recorded at λ_{ex} = 632.8 nm using a near-diffraction focused beam and a nanomolar concentration of the probe molecule. (a) Contour plot of Raman intensity as a function of time (the spectral wavelength range is shown approximately by the region highlighted in the yellow region in Figure 2c using spectral acquisition time of 50 ms). The vertical line profiles show the reproducibility of the SERS signature of RhB over 30 s (the yellow profile shows the reproducibility of the SERS signature at 1350 cm^{-1}; the purple profile shows the reproducibility of the SERS signature at 1275 cm^{-1}; the orange profile shows the reproducibility of the SERS signature at 1200 cm^{-1}). The average (red) and sum (blue) of all spectra show excellent spectral agreement in the peak position and relative intensities with SERS spectra of RhB recorded using high concentrations. The variance (green) in the spectral wavelength and intensity from the blinking Raman spectra is also shown. (b) log–log plot of Raman intensity vs on and off-times (derived from (a)). Inset shows a plot of Raman intensity as a function of time.

strain leading to swelling of the LD regions.[21] The AFM topography image (Figure 1e) of two microarrays of the Au-PPELN surface shows that the arrays consist of a closely packed arrangement of Au nanoparticles. The deposition coverage was nonuniform over the arrays, e.g., the highest Au coverage occurred at the edges of the RIE regions (as shown in Figure

DOI: 10.1021/acsomega.7b01285
ACS Omega 2018, 3, 3165−3172

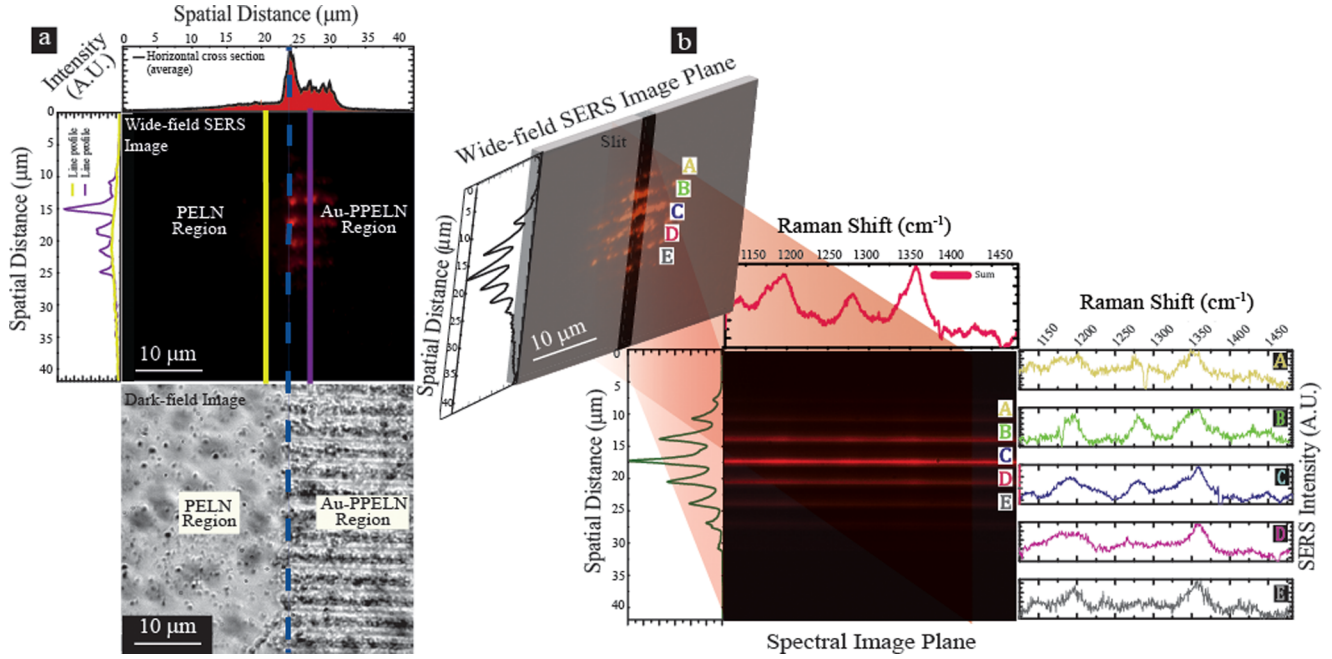

Figure 4. Nonresonant SERS from Au-PPELN with a nanomolar RhB concentration using an expanded excitation laser spot, λ_{ex} = 632.8 nm. (a) SERS and dark-field imaging recorded at the same sample area. The nonresonant SERS image (top) shows red stripelike features that are areas of high SERS intensity. A dark-field image (below) of the same sample area shows the presence of stripelike features assigned to Au (on the right side of the image), whereas to the left is an area of the sample corresponding to where there is no Au deposited on the PPELN surface. The Raman spectrum is clearly seen on the sample on areas where Au nanoparticles are photodeposited. (b) SERS image (top) from an area of the sample where Au nanoparticle microarrays are present over the entire excitation area. The SERS image shows the presence of over six Au microstructured stripelike features (labeled (A)−(E)) that possess SERS intensity distributions. A slit of width 2.5 μm was placed in front of the image, and light was dispersed using a grating. The dispersed SERS spectral image (lower) shows several lines replicating SERS arising from different linear Au stripe positions, labeled (A)−(E). The sum of the SERS spectra from the entire image is shown in the top panel (red spectrum, labeled sum, which is the total sum of SERS spectra from each of five different Au microarray stripes, (A)−(E) confirming that the Raman is from the probe molecule).

1d,f), in line with a previous report.[20] The average height of the deposited Au nanoparticle layer was determined to be 40.00 ± 4.23 nm by subtracting line profiles (n = 10) before and after deposition. Measurements of 10 Au particles located on the PPELN surface reveal that the height of individual nanoparticles is 20.40 ± 7.60 nm, whereas the width is 135.20 ± 29.60 nm as a result of tip broadening. Analysis of the AFM topography images shows that the surface roughness (root mean square of 1.38 μm × 1.38 μm areas (n = 4)) of the LN and LD regions remains unchanged following Au deposition: 2.07 ± 1.06 and 0.75 ± 0.21 nm, respectively, before deposition and 2.46 ± 0.95 and 0.69 ± 0.19 nm, respectively, after Au deposition. The roughness values are significantly increased for the RIE regions from 2.40 ± 0.86 to 8.79 ± 1.89 nm, as a result of the Au deposition.

Optical scattering spectra recorded for the Au-PPELN substrate (Figure 2a) showed a broad band centered at 650 nm. Rhodamine B (RhB) possesses an absorption band located at 550 nm (Figure 2a). Nonresonant Stokes-shifted Raman scattering of RhB occurs when using a 632.8 nm excitation wavelength (λ_{ex}), which overlaps with the surface plasmon resonance wavelength of Au nanoparticles, resulting in nonresonant SERS. The Stokes-shifted Raman scattering of RhB is spectrally separated from the fluorescence of the probe molecule (centered at ca. 575 nm) (Figure 2a).

The interaction between Au nanoparticles and the probe molecule was investigated by fluorescence lifetime imaging and spectroscopy using 470 nm excitation (Figures 2b and S3, Supporting Information). A strong fluorescence enhancement and a shortened lifetime (τ = 2.2 ns) were found for the Au-PPELN substrate with RhB compared to that in PPELN with RhB without Au nanoparticles (τ = 3.5 ns), as shown in Figure 2b.

The Raman scattering spectrum of Au-PPELN with the probe molecule RhB present (Figure 2c) shows several strong Raman scattering bands located between 1100 and 1800 cm^{-1}. These bands are assigned to the probe molecule, as Raman bands arising from PPELN occur only below 1000 cm^{-1}.[11,31−33] The Raman scattering spectrum for the probe molecule on the PPELN surface without Au nanoparticles is characterized by the absence of Raman peaks for RhB (Figure 2c). The absence of RhB Raman peaks indicates that the Au nanoparticles enhance the Raman scattering through plasmon enhancement.[34,35] This confirms that the SERS signal originates in RIE regions where Au nanoparticles have been deposited. The SERS intensity of the three characteristic RhB peaks in the yellow-shaded region (Figure 2c) was determined to vary <7.5% across the Au-PPELN sample (n = 10 locations).

A near-diffraction limit spot size (λ_{ex} = 632.8 nm, confocal volume 0.8 fL) was then used to focus the excitation beam onto a small region (<1 μm in diameter) of a single Au microarray (Figure S4, Supporting Information). A selection of SERS spectra recorded sequentially every 50 ms using a nanomolar RhB concentration (Figure 3a) showed an SERS spectral blinking behavior, e.g., random SERS intensity fluctuations in band position and intensity. Averaging the spectra over the entire time sequence produces a SERS spectrum with the same spectral features as those observed in SERS and Raman spectra of the probe molecule recorded at higher concentrations

DOI: 10.1021/acsomega.7b01285
ACS Omega 2018, 3, 3165−3172

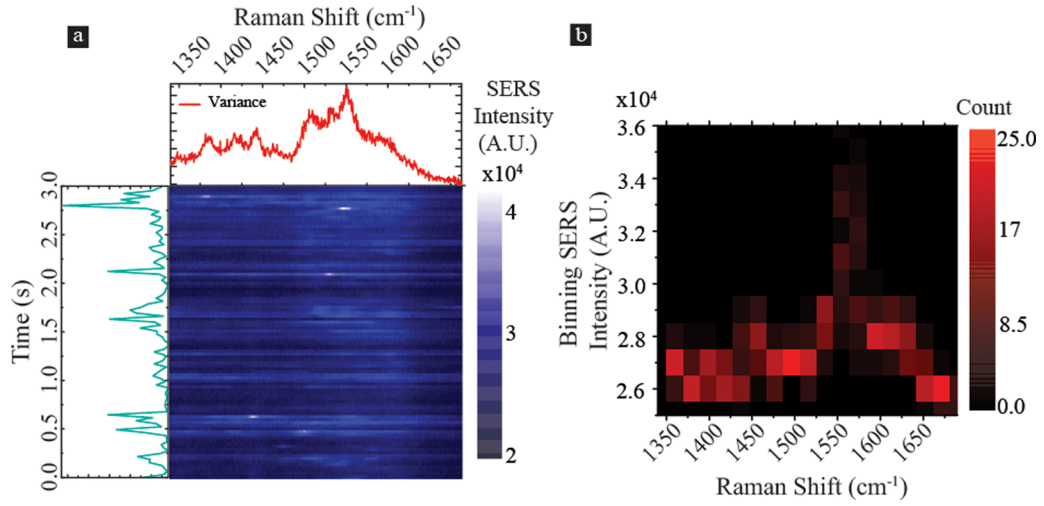

Figure 5. Nonresonant single-molecule SERS from Au-PPELN with a femtomolar RhB concentration using an expanded excitation laser spot, λ_{ex} = 632.8 nm. (a) Contour plot of Raman intensity as a function of time using a spectral acquisition time of 30 ms. The vertical line profile shows the variance of the fluctuation intensity of RhB with femtomolar concentration for 3 s. The SERS spectrum (red) was calculated from the variance of 100 successive SERS spectra shown in the contour plot. (b) The binning intensity as a function of the Raman shift calculated from the contour plot of Raman intensity in (a).

(shown in Figure 2c). This confirms that the spectral blinking arises from the probe molecule.

A series of statistical schemes were applied to examine the SERS blinking, specifically sum (Figure 3a (blue spectrum)), averaging (Figure 3a (red spectrum)), and variance (Figure 3a (green spectrum)). These schemes all show SERS spectra that match the Raman spectrum for RhB. The variance spectrum shows a series of narrow peak widths at full half maxima compared with the average spectrum and the spectrum obtained by summing all of the blinking Raman spectra together (sum spectrum). The observed peak narrowing in the variance spectrum can be potentially applied as an analysis tool for single-molecule Raman spectra in addition to summing and averaging schemes.

The observed blinking (Figure 3a) can be assigned to arise from plasmon-enhanced Raman scattering of single or few RhB molecules. Power-law statistics have been used to measure and analyze single-molecule SERS blinking events.[33,36−38] A log−log plot of the on- and off-times of the blinking Raman intensities is shown in Figure 3b. The plot for the SERS on-time shows a power-law dependence given by $P_{on}(t) = At^{a\text{-on}}$, in line with previous reports for single-molecule SERS.[33,36,37] For the SERS off-time, a truncated power law $P_{off}(t) = At^{a\text{-off}}\, e^{-t/\Gamma}$ fit was applied, where $P_{on,off}(t)$ are the probability distributions of the on and off SERS events for a duration time, t, A is a normalization coefficient, a-on and a-off are power-law exponents for the on and off SERS events, and Γ is the truncation time in the power law.[33,36] The truncation time in the SERS off-time is given by $\Gamma = r/2kBT$, where r is the random walk time to overcome the energy barrier between emissive and nonemissive states.[33,36] This energy barrier may be attributed to a periodic electromagnetic field enhancement at hot spots. The nonzero truncation time obtained from power-law fitting (Figure 3b) suggests the presence of nanoscale plasmonic hot spots on the microarrays where single or few probe molecules are randomly trapped.[33,39,40]

Wide-field nonresonant SERS and dark-field imaging (Figure 4) were used to increase the imaged area of the sample and probe more microarray hot spots. The laser excitation beam was expanded to 13 mm to fill the objective aperture to enable SERS imaging of multiple Au microarrays. Imaging was done for a region of the sample where microarrays end was performed using wide-field nonresonant SERS and dark-field techniques. The SERS image (Figure 4a) shows areas of high intensity in red, which occur within RIE area of the sample where Au nanoparticles have been photoreduced to form Au microarrays. The spatial intensity profiles in the horizontal and vertical directions in the SERS image are shown in the top and left panels of Figure 4a, respectively. The features in the dark-field image in Figure 4a, assigned to the presence of Au nanoparticles, coincide with areas that show high SERS signals. This further supports the conclusion that the SERS signal arises from the Au microarrays present on RIE regions.

A separate area of the sample where the Au microarrays cover the whole excitation area was then imaged. The image shows SERS intensity from multiple Au microarrays (labeled (A)−(E) in Figure 4b). The spatial intensity profiles in the vertical direction of the wide-field SERS image are shown in the left panel of Figure 4b to allow the identification of Au microarrays. In the top panel of Figure 4b, the red spectrum shows the sum of the averaged SERS spectra from each Au microarray (Figure 4b(A)−(E)) to form a SERS spectrum with features in line with those of the Raman spectrum of the probe molecule.

A series of different concentrations was studied ranging from micro- to femtomolar concentrations. SERS images for each concentration were recorded sequentially using a 50 ms acquisition time (Figure S5, Supporting Information). The SERS signal occurred less frequently at lower concentrations of the probe molecule. SERS spectra recorded sequentially every 30 ms using a femtomolar RhB concentration (Figure 5a) also showed a blinking behavior. The variance spectrum over the entire time sequence matches the spectral features for the SERS and Raman spectra of the probe molecule recorded at higher concentrations (shown in Figure 2c). This confirms that the spectral blinking arises from the probe molecule. The binning intensity (Figure 5b) as a function of the Raman shift

DOI: 10.1021/acsomega.7b01285
ACS Omega 2018, 3, 3165−3172

demonstrates that the most dominant peaks (1384 and 1568 cm^{-1}) match those of the Raman spectra for RhB.

The Au-PPELN SERS enhancement factor (EF) was calculated using EF = $(I_{SERS}/N_{Surf})/(I_{RS}/N_{vol})$, where N_{vol} is the average number of molecules in the scattering volume, I_{SERS} is the single-molecule SERS intensity, I_{RS} is the Raman intensity for the same probe molecule, and N_{Surf} is the average number of adsorbed molecules in the scattering volume for the SERS experiments.[40] An average EF of $\sim 1 \times 10^{11}$ was estimated, calculated using EF questions and 1149, 1285, and 1354 cm^{-1} peaks of RhB. The occurrence of such a large EF may be associated the closely packed arrangement of Au nanoparticles on the PPELN surface (Figure 1), which results in conditions that yield small nanoparticle separation distances and high electromagnetic hot spot intensities. The presence of such hot spots likely results in a strong SERS signal, enabling SM detection using normal Raman excitation conditions. Previous COMSOL simulations of line profiles of nanoparticles deposited on PPELN showed evidence for the presence of plasmonic hot spots.[31]

CONCLUSIONS

In conclusion, microarrays of Au nanoparticles were prepared by photodeposition on a periodically proton-exchanged lithium niobate substrate (Au-PPELN). This Au-PPELN substrate is plasmon-active, supporting nonresonant single-molecule Raman spectroscopy at ultralow concentrations ($<10^{-9}$–10^{-13} M), with the substrate supporting a Raman enhancement factor of ca. 10^{11}. The plasmon-active substrates enabled SERS imaging to be performed with low power density ($<1 \times 10^{-3}$ W cm^{-2}) using a wide-field imaging technique. The substrates reported here potentially exhibit Raman enhancement through both electromagnetic enhancement via plasmonic hot spots and chemical enhancement. This high-sensitivity SERS platform can be used to develop substrates for ultra-sensitive analytical sensing applications.

EXPERIMENTAL METHODS

Five hundred micrometers thick $-Z$ cut optical grade congruent LN crystals were used to fabricate PPELN templates, as previously described.[8,20] The selective chemical patterning of the LN surface was conducted by exposing the samples to pure benzoic acid for 24 h at 200 °C through 2.0 μm wide RIE openings in a titanium mask. The titanium mask was subsequently removed by etching in dilute hydrofluoric acid for a few seconds. The resulting periodic pattern at the crystal surface consisted of pure LN and PE stripes, with widths of 0.95 and 5.15 μm, respectively. Prior to photodeposition, the samples were sonicated for 20 min each in acetone, isopropanol, and deionized water before being dried with compressed nitrogen. The PPELN samples were placed on a glass slide, and 150 μL of 0.01 M $HAuCl_4$ (Sigma-Aldrich) was pipetted onto the surface. The samples were illuminated with a 254 nm UV light source (11SC-2, Spectroline) located 2 cm above the surface for 20 min. After illumination, the samples were immersed in deionized water for 1 min and then blown dry with nitrogen. The samples were reused following the cleaning steps described above, with an additional step of gently rubbing the sample with lens paper soaked in isopropanol before the acetone and isopropanol sonication steps. Amplitude modulation atomic force microscopy (AFM) (MFP-3D, Asylum Research) was used to probe the surface topography of each sample before and after photodeposition with PPP-NCH cantilevers having a typical resonant frequency of ~310 kHz and spring constant of ~40 N m^{-1} (nanosensors).

Rhodamine B (RhB) was used as a probe molecule to investigate the plasmonic properties of the Au microarrays. RhB was deposited by immersing the sample in different aqueous concentrations of RhB for 24 h, followed by dipping in deionized water for 5 min to wash off any excess probe molecules. Microspectroscopy instrumentation (Figure S1, Supporting Information) consisting of a spectrograph (IsoPlane 630) attached to a back-illuminated EMCCD (ProEM-HS) 512BX3 charge-coupled device (CCD) camera and a microscope (Olympus IX71) was used to acquire Raman spectra, fluorescence spectra, and fluorescence images. Wide-field SERS imaging experiments were implemented using a homemade telescope system designed for a 632.8 nm wavelength and attached to the illumination port of the microscope. The samples were illuminated through a 100× 0.8 NA objective. Employing wide-field illumination with a spot diameter of ~40 μm and a pixel density of 247 × 247 pixels, integration time was 3–30 s, with 30–50 ms acquisition times. The excitation laser power density was <0.08 MW cm^{-2}, and the spatial resolution was 116 nm per pixel.

Fluorescence lifetime experiments were conducted using a 470 nm excitation laser and millimolar concentration of RhB, whereas the fluorescence imaging studies were established by using 470 and 532 nm excitation lasers with a millimolar concentration of RhB. The microscope was also equipped with two single-photon counting avalanche photodiodes with a Hanbury Brown–Twiss configuration for time-resolved measurements.[28−30] All data acquisition, dark-field images, fluorescence images, and wide-field SERS images were constructed using LightField software (Princeton Instruments, version 5.3). Data processing, such as averaging, summing, variance, data binning, and generating contour plots, were performed using codes written in MATLAB (MathWorks, version 16a).

ASSOCIATED CONTENT

Supporting Information

The Supporting Information is available free of charge on the ACS Publications website at DOI: 10.1021/acsomega.7b01285.

A schematic of the microspectroscopy instrumentation, AFM images of $-Z$ PPELN and X-cut LN before and after Au deposition and fluorescence images of RhB on these samples; the optical scattering, absorption, and emission spectra from the Au-PPELN substrate; Raman spectra of PPELN-RhB and Au-PPELN-RhB recorded at 532, 470, and 632.8 nm; fluorescence images recorded at 532 and 470 nm for PPELN-RhB with and without Au nanoparticles; a wide-field SERS image of the Au-PPELN substrate with a 1 nM RhB concentration, a zoom-in of a confocal image showing a single hot spot and corresponding on and off SERS spectra for a single hot spot acquired using a CCD camera; Raman intensity traces acquired from the confocal volume indicated using an avalanche photodiode and concentration dependence of wide-field SERS imaging (PDF)

AUTHOR INFORMATION

Corresponding Authors

*E-mail: nebras.alattar@ucd.ie (N.A.).
*E-mail: brian.rodriguez@ucd.ie (B.J.R.).

DOI: 10.1021/acsomega.7b01285
ACS Omega 2018, 3, 3165−3172

*E-mail: james.rice@ucd.ie (J.H.R.).

ORCID

Rusul M. Al-Shammari: 0000-0002-7214-1457
Nebras Al-attar: 0000-0002-4669-4648
Brian J. Rodriguez: 0000-0001-9419-2717
James H. Rice: 0000-0002-1035-5708

Notes

The authors declare no competing financial interest.

■ ACKNOWLEDGMENTS

This publication has emanated from research conducted with the financial support of the UCD School of Physics. This work was also supported by the Swedish Scientific Research Council (VR 622-2010-526 and 621-2011-4040) and the ADOPT Linnaeus Centre for Advanced Optics and Photonics in Stockholm. The AFM and the Raman system used for this work were funded by the Science Foundation, Ireland, (SFI07/IN1/B931) and (SFI12/IP/1556), respectively. The authors are grateful to Dr. Aoife Gowen for access to the scattering measurement system.

■ REFERENCES

(1) Rankin, C.; Chou, C.-H.; Conklin, D.; Bonnell, D. A. Polarization and local reactivity on organic ferroelectric surfaces: ferroelectric nanolithography using poly (vinylidene fluoride). *ACS Nano* **2007**, *1*, 234−238.

(2) Grammatikopoulos, P.; Steinhauer, S.; Vernieres, J.; Singh, V.; Sowwan, M. Nanoparticle design by gas-phase synthesis. *Adv. Phys.: X* **2016**, *1*, 81−100.

(3) Qian, X. M.; Nie, S. M. Single-molecule and single-nanoparticle SERS: from fundamental mechanisms to biomedical applications. *Chem. Soc. Rev.* **2008**, *37*, 912−920.

(4) Liu, X.; Kitamura, K.; Yu, Q.; Xu, J.; Osada, M.; Takahiro, N.; Li, J.; Cao, G. Tunable and highly reproducible surface-enhanced Raman scattering substrates made from large-scale nanoparticle arrays based on periodically poled $LiNbO_3$ templates. *Sci. Technol. Adv. Mater.* **2013**, *14*, No. 055011.

(5) Liu, X.; Kitamura, K.; Terabe, K.; Hatano, H.; Ohashi, N. Photocatalytic nanoparticle deposition on $LiNbO_3$ nanodomain patterns via photovoltaic effect. *Appl. Phys. Lett.* **2007**, *91*, No. 044101.

(6) Hanson, J. N. Domain Patterned Ferroelectric Surfaces for Selective Deposition via Photochemical Reaction. Ph.D. Thesis, North Carolina State University, 2007.

(7) Dehong, H.; Zi Jie, C.; Yilun, S.; John, H.; Yan, Z. Diamond micro-milling of lithium niobate for sensing applications. *J. Micromech. Microeng.* **2016**, *26*, No. 095005.

(8) Carville, N. C.; Manzo, M.; Damm, S.; Castiella, M.; Collins, L.; Denning, D.; Weber, S. A. L.; Gallo, K.; Rice, J. H.; Rodriguez, B. J. Photoreduction of SERS-active metallic nanostructures on chemically patterned ferroelectric crystals. *ACS Nano* **2012**, *6*, 7373−7380.

(9) Mailis, S. UV laser induced ferroelectric domain inversion in lithium niobate single crystals. *J. Opt.* **2010**, *12*, No. 095601.

(10) Balobaid, L.; Carville, N. C.; Manzo, M.; Collins, L.; Gallo, K.; Rodriguez, B. J. Photoreduction of metal nanostructures on periodically proton exchanged MgO-doped lithium niobate crystals. *Appl. Phys. Lett.* **2013**, *103*, No. 182904.

(11) Damm, S.; Carville, N. C.; Manzo, M.; Gallo, K.; Lopez, S. G.; Keyes, T. E.; Forster, R. J.; Rodriguez, B. J.; Rice, J. H. Surface enhanced luminescence and Raman scattering from ferroelectrically defined Ag nanopatterned arrays. *Appl. Phys. Lett.* **2013**, *103*, No. 083105.

(12) Neumayer, S. M.; Ivanov, I. N.; Manzo, M.; Kholkin, A. L.; Gallo, K.; Rodriguez, B. J. Interface and thickness dependent domain switching and stability in Mg doped lithium niobate. *J. Appl. Phys.* **2015**, *118*, No. 224101.

(13) Esseling, M.; Zaltron, A.; Sada, C.; Denz, C. Charge sensor and particle trap based on z-cut lithium niobate. *Appl. Phys. Lett.* **2013**, *103*, No. 061115.

(14) Liu, X.; Kitamura, K.; Terabe, K.; Zeng, H.; Yin, Q. Effect of nonstoichiometric defects on antiparallel domain formation in $LiNbO_3$. *Appl. Phys. Lett.* **2007**, *91*, No. 232913.

(15) Sun, Y.; Eller, B. S.; Nemanich, R. J. Photo-induced Ag deposition on periodically poled lithium niobate: Concentration and intensity dependence. *J. Appl. Phys.* **2011**, *110*, No. 084303.

(16) Bryan, D. A.; Gerson, R.; Tomaschke, H. E. Increased optical damage resistance in lithium niobate. *Appl. Phys. Lett.* **1984**, *44*, 847−849.

(17) Kilinc, D.; Blasiak, A.; Baghban, M. A.; Carville, N. C.; Al-Adli, A.; Al-Shammari, R. M.; Rice, J. H.; Lee, G. U.; Gallo, K.; Rodriguez, B. J. Charge and topography patterned lithium niobate provides physical cues to fluidically isolated cortical axons. *Appl. Phys. Lett.* **2017**, *110*, No. 053702.

(18) Carville, N. C.; Collins, L.; Manzo, M.; Gallo, K.; Lukasz, B. I.; McKayed, K. K.; Simpson, J. C.; Rodriguez, B. J. Biocompatibility of ferroelectric lithium niobate and the influence of polarization charge on osteoblast proliferation and function. *J. Biomed. Mater. Res., Part A* **2015**, *103*, 2540−2548.

(19) Arizmendi, L. Photonic applications of lithium niobate crystals. *Phys. Status Solidi A* **2004**, *201*, 253−283.

(20) Carville, N. C.; Neumayer, S. M.; Manzo, M.; Gallo, K.; Rodriguez, B. J. Biocompatible Gold nanoparticle arrays photo-deposited on periodically proton exchanged lithium niobate. *ACS Biomater. Sci. Eng.* **2016**, *2*, 1351−1356.

(21) Manzo, M.; Laurell, F.; Pasiskevicius, V.; Gallo, K. Electrostatic control of the domain switching dynamics in congruent $LiNbO_3$ via periodic proton-exchange. *Appl. Phys. Lett.* **2011**, *98*, 16−19.

(22) Al-Shammari, R. M.; Manzo, M.; Gallo, K.; Rice, J. H.; Rodriguez, B. J. Tunable wettability of ferroelectric lithium niobate surfaces: The role of engineered microstructure and tailored metallic nanostructures. *J. Phys. Chem. C* **2017**, *121*, 6643−6649.

(23) Mallia, R. J.; McVeigh, P. Z.; Veilleux, I.; Wilson, B. C. Filter-based method for background removal in high-sensitivity wide-field-surface-enhanced Raman scattering imaging in vivo. *J. Biomed. Opt.* **2012**, *17*, No. 076017.

(24) Bohndiek, S. E.; Wagadarikar, A.; Zavaleta, C. L.; Van de Sompel, D.; Garai, E.; Jokerst, J. V.; Yazdanfar, S.; Gambhir, S. S. A small animal Raman instrument for rapid, wide-area, spectroscopic imaging. *Proc. Natl. Acad. Sci. U.S.A.* **2013**, *110*, 12408−12413.

(25) Hanson, J. N.; Rodriguez, B. J.; Nemanich, R. J.; Gruverman, A. Fabrication of metallic nanowires on a ferroelectric template via photochemical reaction. *Nanotechnology* **2006**, *17*, 4946.

(26) Blackie, E. J.; Le Ru, E. C.; Etchegoin, P. G. Single-molecule surface-enhanced Raman spectroscopy of nonresonant molecules. *J. Am. Chem. Soc.* **2009**, *131*, 14466−14472.

(27) Le Ru, E. C.; Etchegoin, P. G. Single-molecule surface-enhanced Raman spectroscopy. *Annu. Rev. Phys. Chem.* **2012**, *63*, 65−87.

(28) Al-Attar, N.; Kennedy, E.; Kelly, G.; Rice, J. H. Photo-luminescence blinking from single CdSeS/ZnS quantum dots in a conducting polymer matrix. *J. Phys. Chem. C* **2015**, *119*, 6278−6287.

(29) Al-Attar, N.; Kopf, I.; Kennedy, E.; Flavin, K.; Giordani, S.; Rice, J. H. Surface-enhanced Raman scattering from small numbers of purified and oxidised single-walled carbon nanotubes. *Chem. Phys. Lett.* **2012**, *535*, 146−151.

(30) Al-Alttar, N.; Kopf, I.; Flavin, K.; Kennedy, E.; Giordani, S.; Rice, J. H. Surface-enhanced Raman scattering spectra of radial breathing and G band modes in functionalised nanotubes. *Chem. Phys. Lett.* **2013**, *568*−*569*, 95−100.

(31) Damm, S.; Carville, N. C.; Rodriguez, B. J.; Manzo, M.; Gallo, K.; Rice, J. H. Plasmon enhanced Raman from Ag nanopatterns made using periodically poled lithium niobate and periodically proton exchanged template methods. *J. Phys. Chem. C* **2012**, *116*, 26543−26550.

DOI: 10.1021/acsomega.7b01285
ACS Omega 2018, 3, 3165−3172

(32) Sidorov, N. V.; Syuy, A. V.; Palatnikov, M. N.; Evstratova, D. V.; Mavrin, B. N. Photorefractive and Raman light scattering in lithium niobate ferroelectric crystal. *Opt. Spectrosc.* **2011**, *110*, 864−870.
(33) Kitahama, Y.; Araki, D.; Yamamoto, Y. S.; Itoh, T.; Ozaki, Y. Different behaviour of molecules in dark SERS state on colloidal Ag nanoparticles estimated by truncated power law analysis of blinking SERS. *Phys. Chem. Chem. Phys.* **2015**, *17*, 21204−21210.
(34) Ding, S.-Y.; Yi, J.; Li, J.-F.; Ren, B.; Wu, D.-Y.; Panneerselvam, R.; Tian, Z.-Q. Nanostructure-based plasmon-enhanced Raman spectroscopy for surface analysis of materials. *Nat. Rev. Mater.* **2016**, *1*, No. 16021.
(35) Lin, K.-Q.; Yi, J.; Hu, S.; Liu, B.-J.; Liu, J.-Y.; Wang, X.; Ren, B. Size effect on SERS of gold nanorods demonstrated via single nanoparticle spectroscopy. *J. Phys. Chem. C* **2016**, *120*, 20806−20813.
(36) Cichos, F.; Vonborczyskowski, C.; Orrit, M. Power-law intermittency of single emitters. *Curr. Opin. Colloid Interface Sci.* **2007**, *12*, 272−284.
(37) Kneipp, K.; Moskovits, M.; Kneipp, H. *Surface-Enhanced Raman Scattering*; Springer: Berlin, 2006.
(38) Etchegoin, P. G.; Meyer, M.; Le Ru, E. C. Statistics of single molecule SERS signals: is there a Poisson distribution of intensities? *Phys. Chem. Chem. Phys.* **2007**, *9* (23), 3006−3010.
(39) Kitahama, Y.; Enogaki, A.; Tanaka, Y.; Itoh, T.; Ozaki, Y. Truncated power law analysis of blinking SERS of thiacyanine molecules adsorbed on single silver nanoaggregates by excitation at various wavelengths. *J. Phys. Chem. C* **2013**, *117*, 9397−9403.
(40) Le Ru, E. C.; Blackie, E.; Meyer, M.; Etchegoin, P. G. Surface enhanced Raman scattering enhancement factors: A Comprehensive Study. *J. Phys. Chem. C* **2007**, *111*, 13794−13803.

DOI: 10.1021/acsomega.7b01285
ACS Omega 2018, 3, 3165−3172